Local Ca-Mg distribution of Mg-rich pyrope-grossular garnets synthesized at different temperatures revealed by 29Si MAS NMR spectroscopy

Article *in* American Mineralogist · September 1999

DOI: 10.2138/am-1999-0921

CITATIONS
33

READS
100

3 authors, including:

Charles A. Geiger
University of Salzburg

239 PUBLICATIONS **4,184** CITATIONS

SEE PROFILE

American Mineralogist, Volume 84, pages 1422–1432, 1999

Local Ca-Mg distribution of Mg-rich pyrope-grossular garnets synthesized at different temperatures revealed by ^{29}Si MAS NMR spectroscopy

ANNE BOSENICK,[1,*] CHARLES A. GEIGER,[1] AND BRIAN L. PHILLIPS[2]

[1]Institut für Geowissenschaften, Christian-Albrechts-Universität zu Kiel, Olshausenstrasse 40, 24098 Kiel, Germany
[2]Department of Chemical Engineering and Materials Science, University of California, Davis, California 95616, U.S.A.

ABSTRACT

Pyrope-grossular solid solutions, $(Mg,Ca)_3Al_2Si_3O_{12}$, of composition $Py_{85}Gr_{15}$ and $Py_{75}Gr_{25}$ were synthesized at 1000, 1200, and 1400 °C and 30 kbars in a piston-cylinder device. The synthetic garnets were characterized using optical, microprobe, and X-ray methods and their Ca-Mg distributions were investigated using ^{29}Si MAS NMR spectroscopy. The syntheses produced 100% garnet except for those undertaken at 1000 °C, where small amounts (up to 3%) of clinopyroxene were present. X-ray powder refinements showed differences up to 0.01 Å in the unit-cell dimension of the garnets synthesized at the three different temperatures. A general decrease of the X-ray diffraction line widths with increasing synthesis temperature is observed. The ^{29}Si NMR spectra of $Py_{85}Gr_{15}$ show little change as a function of synthesis temperature. In the spectra of $Py_{75}Gr_{25}$ small but measurable changes in the relative peak intensities, depending upon synthesis temperature, were observed with a more random cation distribution corresponding to a higher synthesis temperature. None of the garnets investigated has a completely random Ca-Mg distribution. The reduction in configurational entropy compared to the disordered state is estimated to be less than 2 J/mol·K.

INTRODUCTION

Aluminosilicate garnet solid solutions ($X_3^{[8]}Al_2^{[6]}Si_3^{[4]}O_{12}$, with X = Fe^{2+}, Mn^{2+}, Mg, and Ca) are considered to have complete random distributions of cations on the X-site. However, ^{29}Si MAS NMR spectroscopic study of synthetic garnets along the pyrope-grossular join (Bosenick et al. 1995) demonstrated the presence of short-range order of Mg and Ca in intermediate compositions ($0.85 \geq X_{Mg} \geq 0.25$). The pyrope-grossular garnets were largely synthesized over a limited temperature range (1050–1150 °C). Hence the degree of ordering, which is temperature dependent, could only be investigated at the simplest level. The results of our original study, if correct, require that the configurational entropies for such garnets will differ from those calculated assuming complete random disorder (i.e., $S^{conf} = -3R\cdot[X_{Ca}\ln(X_{Ca}) + X_{Mg}\ln(X_{Mg})]$. Hence, the thermodynamic modeling previously undertaken on pyrope-grossular garnets would have to be revised.

We extended our original study by synthesizing two pyrope-rich compositions, namely $Py_{85}Gr_{15}$ and $Py_{75}Gr_{25}$, at three temperatures 1000, 1200, and 1400 °C to test whether short-range order can be quenched in from high pressures and temperatures and measured by ^{29}Si NMR spectroscopy. If so, the temperature dependence and some idea behind the energetics of cation ordering in garnets may be gathered. Pyrope-rich compositions were chosen for study, because they are the most important for garnets in the CMAS system and for natural high-pressure garnets, such as those found in grospydites (Sobolev et al. 1968).

*Present address: Department of Earth Sciences, University of Cambridge, Downing Street, Cambridge, CB2 3EQ, England. E-mail: Bosenick@esc.cam.ac.uk

EXPERIMENTAL METHODS

Synthesis and characterization

Garnets of composition $Py_{85}Gr_{15}$ and $Py_{75}Gr_{25}$ were synthesized from homogeneous glasses at high pressures and temperatures in a piston-cylinder device. The following oxides were used to prepare the glasses: Al_2O_3 [Johnson Mattey (JM), ALFA Products, 99.99%], $CaCO_3$ (JM, ultrapure), MgO (JM, puratronic powder) and SiO_2 (JM, 99.999%). The preparation of the oxide mixtures (between 5 and 6 g) and the synthesis methods of the glasses were similar to those described in Bosenick et al. (1995), except that the glasses were melted at 1650 °C for a total of 60 min, instead of 30 min. In addition, the glasses were ground and remelted twice to ensure compositional homogeneity. From each of the first two meltings about 1.5 g of the obtained glass was separated and reserved for syntheses. At the end of the procedure, between 2 and 3 g of glass were obtained which had been melted a total of three times. The first melting experiment produced better than 99% glass, which increased in the second and third melting procedure. Microprobe analysis of the final glasses showed them to be homogeneous within better than 1% ($\pm 1\sigma$) of their average composition. No changes in composition were observed between the glasses obtained from the different melting cycles. The measured pyrope mole fractions of the glasses were X_{Mg} = 0.847(4) and X_{Mg} = 0.746(4).

The *P-T* synthesis conditions of the pyrope-grossular garnets are summarized in Table 1. Between 180 and 220 mg of starting glass material and about 1 μL of distilled water were sealed in 5.0 mm diameter Pt or Au capsules. The syntheses were undertaken in 1/2 inch talc-glass assemblies at a corrected pressure of 30 ± 0.5 kbars, which accounts for a friction correc-

0003-004X/99/0009–1422$05.00

tion of 18% (M. Rauch, personal communication). Thermal gradients over the capsule length are estimated to be less than 15 °C with the tapered furnace used. The experiments were quenched to room temperature by switching off the power. Not more than 15 s were needed to quench the samples to 800 from 1400 °C. About 10 and 5 s were needed to quench them to 800 °C from 1200 and 1000 °C, respectively. The polycrystalline garnet products were characterized by optical microscopy, electron microprobe, and powder X-ray diffraction analysis. The garnets were optically isotropic with the size of the crystallites being between 10 and 30 μm. The samples B001 and B003 (i.e., synthesis of $Py_{75}Gr_{25}$ and $Py_{85}Gr_{15}$ at 1000 °C) showed small amounts (less than 3%) of a second phase identified as clinopyroxene by X-ray diffraction. The syntheses undertaken at 1200 and 1400 °C produced only garnet.

The garnets were analyzed with a Cameca Camebax microprobe with an acceleration voltage of 15 kV and a beam current of 30 mA using common oxides and silicates as standards. The diameter of the electron beam was approximately 1 μm. Each spot was measured for 20 s and the background for 10 s. The mean compositions expressed as the pyrope mole fraction, determined from about 15 spot analyses, are given in Table 1. The results of the microprobe analysis showed that the garnets were homogeneous within 1% ($\pm 1\sigma$) of the average composition. A complete list of the microprobe analyses is on deposit.[1]

All garnets were also characterized with an automated powder X-ray diffractometer (Siemens D5000) using Cu$K\alpha$ radiation. The diffraction patterns were collected in step-scanning mode from 10 to 130° 2θ using 0.01° 2θ increments and 4 seconds counting time per step. The unit-cell parameter, a_0, was calculated from the powder diffraction data by least-squares refinement with the program PULVER91 (Weber 1991). To retain as much material as possible for the NMR measurements, the powder X-ray refinements were made using an external Si standard (NBS 640b). Repeated measurements of the Si standard during the period of the X-ray measurements revealed no changes in the measuring conditions. The results of the unit-cell refinements are given in Table 1.

It has to be emphasized that although water was meant to be used as a flux in the synthesis experiments of our garnets, they do incorporate some trace amouts of OH^-. Such amounts will not have a measureable effect on the physical properties such as lattice constant or the conclusions drawn from NMR spectra. This conclusion is based on the following: (1) Experimental studies by Ackermann et al. (1983), Geiger et al. (1991) and Withers et al. (1998) have shown that at *P-T* conditions similar to our synthesis experiments not more than 0.05 wt% of H_2O can be incorporated in pyrope or grossular. The three former studies were done under water saturated conditions with $P(H_2O) = P(\text{total})$ using a liquid-to-solid ratio between 1 to 4 and 1 to 10. Our syntheses were done using much less water. Here the liquid to solid ratio is a factor of 20 to 50 smaller. Any incorporation of OH^- into our garnets should therefore be at least one order of magnitude smaller, i.e., much less than 0.005 wt% H_2O. (2) IR measurements were undertaken on polycrystalline garnet chips of 100 to 300 μm thicknesses using a Bruker IFS66V spectrometer equipped with a microscope. No evidence for the incorporation of OH^- was found, i.e., no OH^--bands are observable at about 3630 cm^{-1}. Using the background level in the spectrum as maximum peak height, the maximum water content possible is estimated to be well below 0.01 wt% H_2O. (3) The inflation of the lattice constant due to the incorporation of trace amounts of OH^- will be very small. Geiger et al. (1991) showed that 0.05 wt% H_2O in pyrope produces an increase in the lattice constant ranging from 0.002 to 0.004 Å. According to the study by Cheng et al. (1990), the expansion of the lattice constant of grossular due to 0.05 wt% H_2O would be less than 0.002 Å. Our garnets have water contents which are at least one order of magnitude smaller and hence, the effect on the lattice constant would be even smaller. (4) Assuming a "water" content of 0.005 wt% held in the hydrogarnet substitution, if follows that only 0.04% of the ^{29}Si nuclei could be replaced by H. This will have no measurable influence on the NMR peak intensities with respect to the inherent experimental errors that are discussed below. Moreover, the NMR spectra are in agreeement with those collected previously on OH-free garnets (Bosenick et al. 1995).

^{29}Si MAS NMR spectroscopy

Garnets synthesized under identical conditions, i.e., same *P-T* conditions and same starting glass material, were combined for the ^{29}Si MAS NMR measurements except for the $Py_{85}Gr_{15}$ samples synthesized at 1400 °C, because of observed differences in their unit-cell constants. The samples used for the NMR measurements are listed in Table 1.

The ^{29}Si MAS NMR spectra were measured with a Chemagnetics CMX-400 spectrometer operating at 79.49 MHz. Samples were contained in either 7.5 or 5.0 mm (outside diameter) zirconia rotors and spun at 5.0 kHz. The data were collected by single-pulse excitation consisting of 90° pulses (5–6 μs) and a 300 s interpulse delay for a total of 300–700 acquisitions. This interpulse delay corresponds approximately to the spin-lattice relaxation time measured for sample Py85-1000. We found no significant difference between spectra collected for this sample with 300 s and 30 s recycle delays. We report the chemical shifts relative to tetramethylsilane (0 ppm), measured via a secondary reference sample of kaolinite that gives narrow peaks at –96.8 and –97.5 ppm. This frequency reference was checked before and after the data collection period for each sample, from which the accumulated drift for each spectrum was determined to be less than 0.1 ppm.

We obtained relative intensities for the ^{29}Si NMR peaks by fitting the spectra to a sum of Pseudo-Voigt curves using a computer program that minimizes χ^2 by varying intensity, position, width, and shape of the peaks. This program is based on a Levenberg-Marquardt algorithm (Press et al. 1986). The peak shapes of the different resonances within a given spectrum are variable as described by Bosenick et al. (1995). In the study herein, it was found that the best peak shape for the resonances

[1]For a copy of deposit table, Document AM-99-026, contact the Business Office of the Mineralogical Society of America (see inside front cover of recent issue) for price information. Deposit items may also be available on the American Mineralogist web site (http://www.minsocam.org or curret web address).

having the largest and second largest intensities is near 50% Gaussian and 50% Lorentzian. Changing the peak shape to 100% Lorentzian or 100% Gaussian can modify the relative intensities absolute by ±1% in the case of high and medium intensity peaks (i.e., ≥ 5%) and by ±0.5% for lower intensity peaks. Hence, using a 50% Gaussian and 50% Lorentzian peak shape yields intermediate values for the relative peak intensities.

The lower detection limit of a resonance in the spectra is at least 1% as determined by fitting peaks in the background above –70 ppm and below –80 or –82 ppm for Py85 and Py75, respectively.

A reliable determination of the relative intensities of the two largest peaks at –72.2 and –73.4 ppm is crucial for the interpretation of the spectra. The two peaks are not statistically equivalent: the resonance at –72.2 ppm forms the left side of a manifold of overlapping peaks (and is thus well constrained), while the peak at –73.4 ppm is overlapped on both sides. The possibility of systematic fitting errors does exist. This problem was addressed by adding an artificial peak centered at –71.0 ppm to the experimental spectra with an area of 20 to 30% of the total resonance envelope. These hypothetical spectra were then fitted and it was found that the relative intensities of the two peaks at –72.2 and –73.4 ppm are identical within 0.5% to those determined on the experimental spectra. The total errors in the relative peak intensities, including those due to variation in peak shapes, are ±1–2% for the high and medium intensity peaks and ±0.5–1% for peaks with intensities below ~5%.

Results and Discussion

Powder X-ray diffraction

The unit-cell refinements show small differences between garnets of the same composition, which were synthesized at different temperatures (Table 1). The a_0 values for $Py_{85}Gr_{15}$ range from 11.5120 up to 11.5223 Å. For $Py_{75}Gr_{25}$, the unit-cell dimensions vary between 11.5579 and 11.5662 Å. The unit-cell dimensions of garnets synthesized at the same temperature show smaller differences. For example, the unit-cell values of the six $Py_{85}Gr_{15}$ syntheses made at 1200 °C show a maximum difference of 0.0022 Å and the two syntheses of $Py_{75}Gr_{25}$ at 1200 °C are within 0.0026 Å of one another. However, the difference in the unit-cell dimensions of the two $Py_{85}Gr_{15}$ samples synthesized at 1400 °C is about 0.0043 Å, which is relatively large. We, therefore, repeated the powder-diffraction measurements on both samples taking different sections from the charge. The results were, within error, identical with the first measurements.

The unit-cell dimension of the different $Py_{85}Gr_{15}$ samples appear to decrease with increasing synthesis temperature (Fig. 1a). This relation also holds for a $Py_{85}Gr_{15}$ sample synthesized at 1100 °C (Bosenick et al. 1995) and having a unit-cell constant of 11.521(1) Å and a pyrope-content of X_{Mg} = 0.841(7), which matches the composition of the $Py_{85}Gr_{15}$ garnets synthesized herein. In the case of the $Py_{75}Gr_{25}$ samples, no systematic change in the unit-cell dimension with synthesis temperature is observed. The cell dimension from the syntheses at 1400 and 1200 °C are the same within error, whereas the 1000 °C sample has a cell-dimension about 0.006 Å smaller than both. This latter synthesis contains, as stated above, small amounts of pyroxene and, therefore, it might not have exactly the same composition as those garnets synthesized at 1200 and 1400 °C. Because of its smaller cell-dimension, one would expect that it is more pyrope-rich. As will be discussed below, the ^{29}Si NMR data also suggest a higher pyrope-content. However, the microprobe analysis does not give a more pyrope-rich composition, but instead a slightly lower pyrope content compared to the other $Py_{75}Gr_{25}$ garnets. It is possible that this lower unit-cell dimension is real, since a $Py_{75}Gr_{25}$ sample synthesized at 1100 °C (Bosenick et al. 1995), having a pyrope content of X_{Mg} = 0.734(8), has a comparable unit-cell constant of 11.5578(4) Å (Fig. 1).

The unit-cell parameter of a solid solution is sensitive to small changes in composition and it could be argued, therefore, that the observed differences are compositionally related. There is evidence, however, that differences in a_0 could be due to different structural states. Reasons for this are, first, the same glass starting material was used for all syntheses of the same composition, and the experiments were performed in a closed system. The syntheses above 1000 °C produced 100% garnet, and hence, the garnets must have the same bulk compositions. Indeed, the compositions of the garnets are identical to those of the glass starting materials as revealed by microprobe analysis. Second, the unit-cell parameters of two garnets from the earlier study synthesized at a temperature of 1100 °C are consistent with the present observations. This supports the proposal that different structural states resulting from different synthesis conditions cause changes in a_0.

The errors in the composition have been included in the calculation of the errors in the unit-cell dimension (Fig. 1). Without considering any compositional uncertainty the errors are four to five times smaller. The errors were calculated as follows: to a first approximation, the change in the unit-cell dimension as a function of composition can, for small changes in composition, i.e., $\Delta X_{Mg} \leq 0.01$, be described by a linear function:

$$a = a_0 + m \cdot \Delta X_{Mg} \quad (1)$$

The slope "*m*" has been determined to be 0.423 and 0.427 for $Py_{85}Gr_{15}$ and $Py_{75}Gr_{25}$, respectively, using the unit-cell dimensions of synthetic pyrope-grossular solid solutions (Ganguly et al. 1993 and Bosenick and Geiger 1997). The errors are then given by $s_a = \sqrt{s^2_{a_0} + m^2 \langle s^2_{DX_{Mg}}}$, where σ_{a_0} and $\sigma_{\Delta X_{Mg}}$ are the errors in the unit-cell parameter and composition, respectively (Table 1).

The powder X-ray patterns were also analyzed with respect to the peak width of the diffraction lines. The results show that those samples synthesized at higher temperatures have narrower peaks and a better $K\alpha_1/\alpha_2$ resolution compared to those synthesized at lower temperature. Since the diffraction lines at higher 2θ are of lower intensity and not all samples show well-resolved α_1/α_2 reflections, we determined the peak-width (FWHM) of the diffraction lines 400, 420, 332, and 422 by fitting Gaussian curves to them. These diffraction lines are of high intensity and no α_1/α_2 splitting is observable. A general decrease in FWHM (Table 2) with increasing synthesis temperature is present, except for the $Py_{85}Gr_{15}$ garnets synthesized at 1400 °C, which have the same peak widths as those garnets synthesized at 1200 °C (Fig. 2a). This relation also holds for the garnets synthesized at 1100 °C (Bosenick et al. 1995). Peak

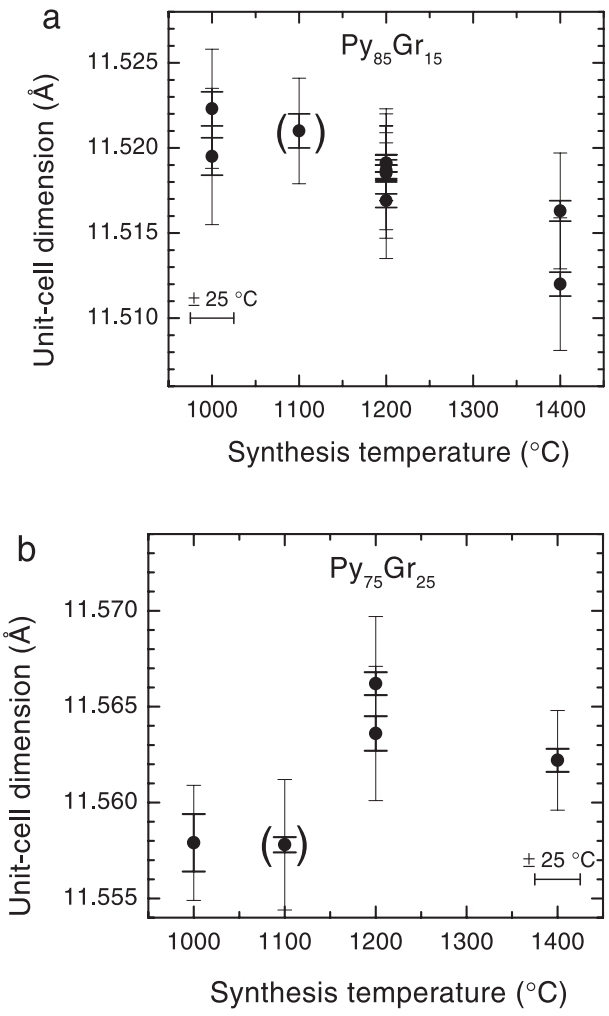

FIGURE 1. Variation of the unit-cell dimension, a_0, as a function of synthesis temperature. (**a**) $Py_{85}Gr_{15}$. (**b**) $Py_{75}Gr_{25}$. The error bars incorporate errors in the unit-cell dimension and composition. Data in parentheses are from Bosenick et al. (1995).

narrowing as a function of synthesis temperature is about two times greater in the $Py_{75}Gr_{25}$ samples than in the $Py_{85}Gr_{15}$ samples.

The initial grain size of the garnet crystallites (10–30 μm), and their size after grinding (about 1–2 μm), is within the range (0.2–10 μm) to produce sharp diffraction lines that should not be affected by crystallite size (e.g., Azaroff and Buerger 1958). Hence, broadening of the diffraction lines must be a result of other physical causes and not particle size. One possible origin is incoherent scattering due to fluctuations in composition and/or structural state over distances comparable to the X-ray scattering length (approximately hundreds of angstroms). Compositional fluctuations on this scale can not be ruled out, because microprobe analysis resolves chemical inhomogeneity only if it has dimensions greater than the excitation volume (2–5 μm).

^{29}Si MAS NMR spectroscopy

For pyrope-grossular garnets, the ^{29}Si NMR chemical shift depends on the local configuration of Ca and Mg in the dodecahedral sites surrounding a SiO_4 tetrahedron. Thus the spectra record the number and distribution of Ca and Mg in the first two coordination shells, where the first shell is formed by the two dodecahedra, which are edge-shared to the SiO_4 tetrahedron, and the second shell is formed by the four dodecahedra, which are corner shared. There are 15 possible and distinct local arrangements of Ca and Mg over these six dodecahedra, which can give rise to an individual NMR resonance. A more detailed description of the problem and complete resonance assignments have been given in Bosenick et al. (1995).

The ^{29}Si MAS NMR spectra herein are similar to those recorded previously. The spectra of samples of composition $Py_{85}Gr_{15}$ contain six resonances with chemical shifts of –72.2, –73.4, –74.5, –75.6, –76.7, and –77.8 ppm (Figs. 3 and 4), which correspond to the configurations MgMg-MgMgMgMg, MgMg-MgMgMgCa, MgMg-MgMgCaCa, MgMg-MgCaCaCa + MgCa-MgMgMgMg, MgMg-CaCaCaCa + MgCa-MgMg MgCa, and MgCa-MgMgCaCa, respectively. (The first two element symbols refer to the cation occupation of the 1st shell and the last four symbols to the occupation of the 2nd shell). In

TABLE 1. Synthesis conditions, compositions, and unit-cell dimensions

Sample	Synthesis temperature (°C)*	Synthesis time (h)	No. of glass meltings	Composition X_{Mg}	Cell dimension a_0 (Å)	NMR-spectra label
			$Py_{85}Gr_{15}$			
B003	1000	18.5	3	0.842 (8)	11.5223 (10)	Py85-1000
B010	1000	17.5	3	0.845 (9)	11.5195 (11)	Py85-1000
B008	1200	13	1	0.849 (5)	11.5191 (5)	Py85-1200a
B019	1200	11	1	0.848 (9)	11.5185 (5)	Py85-1200a
B009	1200	15	2	0.847 (5)	11.5187 (6)	–
B020	1200	11.5	2	0.852 (8)	11.5169 (4)	–
B004	1200	14	3	0.845 (5)	11.5191 (5)	Py85-1200
B016	1200	13.5	3	0.853 (8)	11.5186 (4)	Py85-1200
B005	1400	4	3	0.844 (8)	11.5163 (6)	Py85-1400b
B018	1400	4	3	0.842 (9)	11.5120 (7)	Py85-1400
			$Py_{75}Gr_{25}$			
B001	1000	19	3	0.741 (6)	11.5579 (15)	Py75-1000
B006	1200	12	3	0.749 (8)	11.5662 (6)	Py75-1200
B012	1200	16	3	0.742 (8)	11.5636 (9)	Py75-1200
B007	1400	4	3	0.747 (6)	11.5622 (6)	Py75-1400

* Temperature at the thermocouple which was placed directly above the sample capsule. Because of temperature gradients in the cell, the estimated temperature is considered to be 5 to 20 °C higher.

TABLE 2. Peak widths of selected powder-diffraction lines

Sample	Synthesis T (°C)	Diffraction line (2θ) 400	420	332	422
		$Py_{85}Gr_{15}$			
B003	1000	0.204 (8)	0.224 (9)	0.218 (9)	0.213 (8)
B010	1000	0.203 (7)	0.218 (9)	0.221 (9)	0.221 (9)
R201*	1100	0.197 (7)	0.194 (7)	0.196 (7)	0.195 (7)
B004	1200	0.168 (5)	0.188 (6)	0.188 (6)	0.179 (6)
B016	1200	0.190 (7)	0.199 (7)	0.198 (7)	0.197 (7)
B005	1400	0.190 (7)	0.203 (7)	0.205 (8)	0.200 (7)
B018	1400	0.171 (5)	0.193 (7)	0.193 (7)	0.195 (7)
		$Py_{75}Gr_{25}$			
B001	1000	0.222 (9)	0.238 (10)	0.238 (10)	0.255 (11)
R102*	1100	0.218 (9)	0.224 (9)	0.212 (8)	0.213 (8)
B006	1200	0.200 (7)	0.210 (8)	0.205 (8)	0.205 (8)
B012	1200	0.203 (7)	0.219 (9)	0.216 (8)	0.221 (9)
B007	1400	0.179 (6)	0.187 (6)	0.187 (6)	0.191 (7)

* Samples from Bosenick et al. (1995).

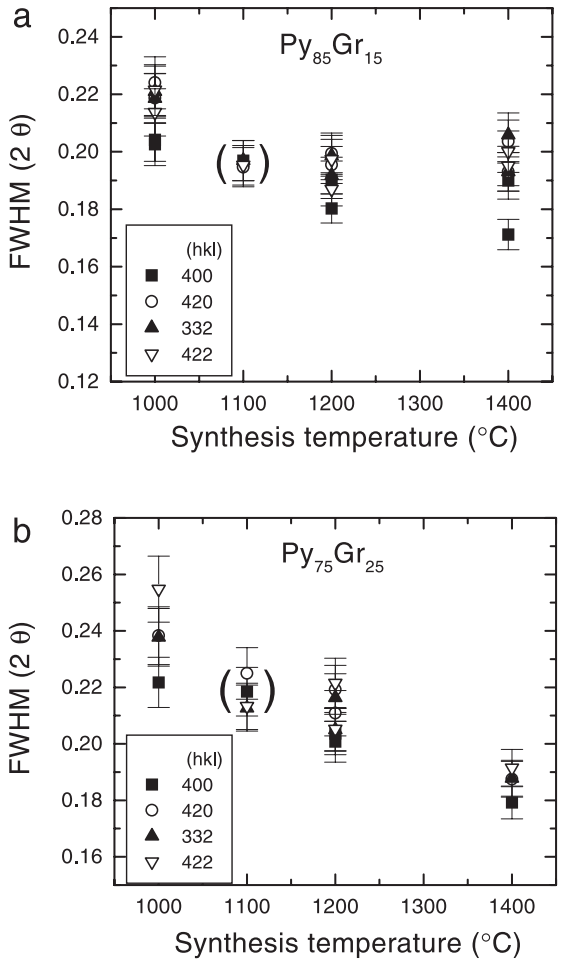

FIGURE 2. Variation of the peak width (FWHM) of the powder X-ray diffraction lines of the reflections 400, 420, 332, and 422 as a function of the synthesis temperature. (**a**) $Py_{85}Gr_{15}$ samples. (**b**) $Py_{75}Gr_{25}$ samples. The data at 1100 °C are from Bosenick et al. (1995).

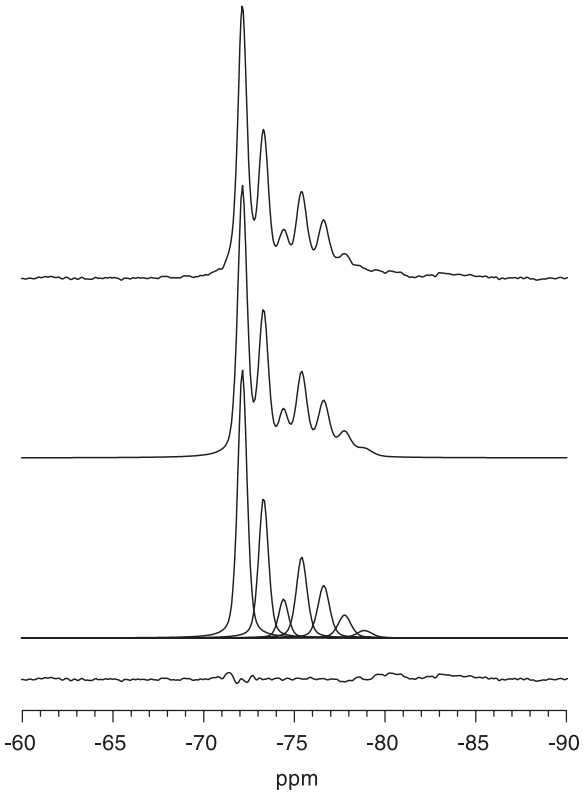

FIGURE 3. ^{29}Si MAS NMR spectrum of $Py_{85}Gr_{15}$ synthesized at 1000 °C. Top, the observed spectrum. Middle, the simulated spectrum, which is the sum of pseudo-Voigt curves shown just below. Bottom line, the difference between the measured and the simulated spectrum.

the spectra of the samples of composition $Py_{75}Gr_{25}$, the same six resonances are observed and, in addition, weak peaks at –78.9 and –80.0 ppm (Fig. 5), which are assigned to the configurations MgCa-MgCaCaCa + CaCa-MgMgMgMg and MgCa-CaCaCaCa + CaCa-MgMgMgCa.

In the spectrum of $Py_{85}Gr_{15}$ synthesized at 1000 °C a small broad peak is observed at about –83.2 ppm (Fig. 3). In the spectrum of $Py_{75}Gr_{25}$ synthesized at 1000 °C a weak broad resonance is present at about –84.3 ppm (Fig. 5). Since grossular shows a ^{29}Si chemical shift at –83.7 ppm and all mixed configurations containing Mg have more positive shifts, the broad resonance in the spectrum Py75-1000 cannot be due to grossular or grossular-rich configurations. Both of these 1000 °C synthesis products have small amounts of pyroxene as revealed by X-ray diffraction, and since the ^{29}Si chemical shift of diopside is about –84.7 ppm (Kirkpatrick et al. 1986), it is possible that both of these resonances are caused by small amounts of pyroxene.

If this is diopside ($CaMgSi_2O_6$) or another pyroxene phase with a higher Ca/Mg ratio or in the extreme case a Mg-free pyroxene phase like Ca-Tschermak ($CaAl_2SiO_6$), it would push the garnet composition towards a higher pyrope content. This change in composition can be estimated from the relative intensity of the possible pyroxene peak, which is about 1% in the spectrum Py85-1000 and 2–3% in the spectrum Py75-1000. If these peaks are from diopside, the composition of $Py_{85}Gr_{15}$

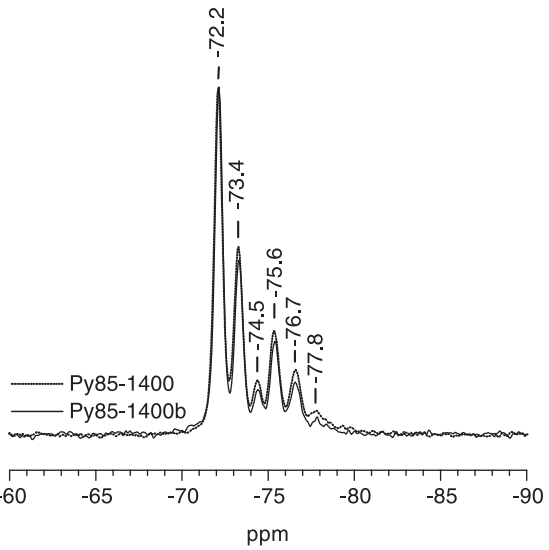

FIGURE 4. ^{29}Si MAS NMR spectra of the two different syntheses of composition $Py_{85}Gr_{15}$ at 1400 °C showing very slight differences in their relative peak intensities. The spectra were normalized to the resonance at –72.2 ppm. The spectra obtained on the other $Py_{85}Gr_{15}$ samples are similar and are, therefore, not shown.

would change by 0.4 mol% to $Py_{85.4}Gr_{14.6}$ and that of $Py_{75}Gr_{25}$ by 1.2 mol% to $Py_{76.2}Gr_{23.8}$. If in the other extreme case the resonances belong to $CaAl_2SiO_6$, the composition of $Py_{85}Gr_{15}$ would change to $Py_{85.8}Gr_{14.2}$ and that of $Py_{75}Gr_{25}$ to $Py_{77.3}Gr_{22.7}$. Hence, some of the differences between the spectra of the samples synthesized at 1000 °C and those synthesized at higher temperatures which will be discussed below, might in part be due to compositional variations in the garnet.

The spectra of the $Py_{85}Gr_{15}$ samples show no major changes in their relative peak intensities as a function of synthesis temperature. Moreover, no differences are observed in the spectra of the garnets synthesized from the different glass starting materials. The largest difference, albeit small, is observed between the two samples synthesized at 1400 °C (Fig. 4). In the case of the spectra of samples with composition $Py_{75}Gr_{25}$ measurable changes in the peak intensities are observed as a function of synthesis temperature. For example, in the spectrum of $Py_{75}Gr_{25}$ synthesized at 1000 °C, the strongest resonance is at –72.2 ppm and the second strongest peak is at –73.4 ppm (Fig. 5). In the spectrum of the sample synthesized at 1200 °C both of these resonances have about the same height and in the spectrum of the garnet synthesized at 1400 °C, the resonance at –73.4 ppm is slightly greater than that at –72.2 ppm.

Table 3 reports the fitting results obtained using 50% Gaussian and 50% Lorentzian curves. The statistical probabilities are the relative intensities calculated for a total random distribution of Mg and Ca over the dodecahedral sites (Bosenick et al. 1995). For a better comparison with the observed intensities, they were normalized so that the sum of the probabilities of the fitted configurations sum up to 100%. These statistical probabilities are given for the composition of the garnet solid-solutions, (1) as determined by microprobe analysis (X_{Mg}^{MP}) and,

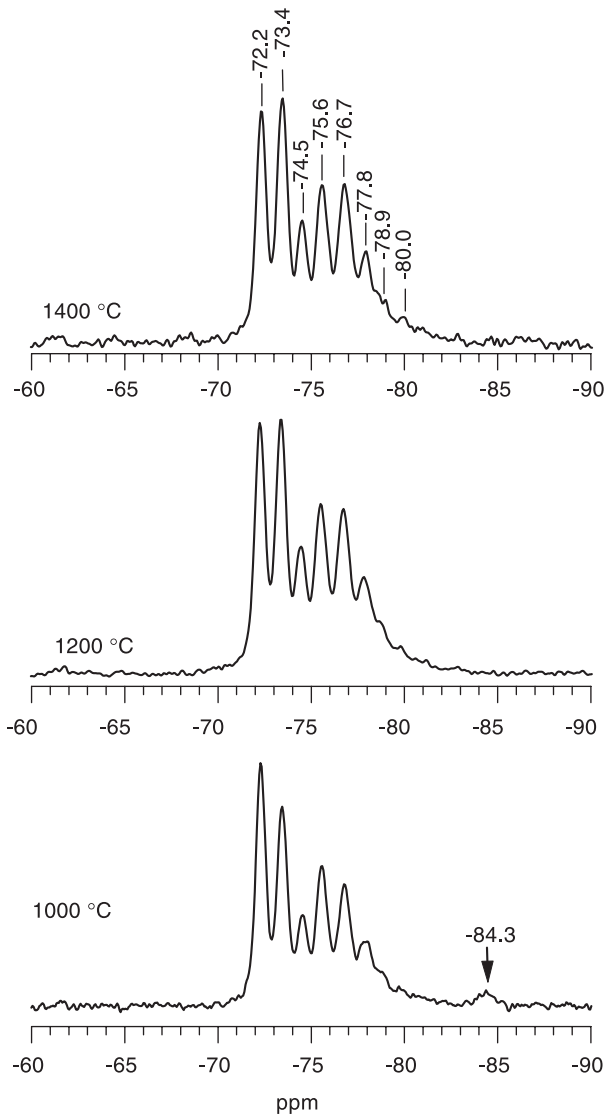

FIGURE 5. ^{29}Si MAS NMR spectra of the $Py_{75}Gr_{25}$ samples synthesized at three different temperatures (1000, 1200, and 1400 °C). All spectra were normalized to display the same height as the resonance at –72.2 ppm.

(2) as computed from the NMR spectra (X_{Mg}^{NMR}). The NMR spectra allow the calculation of the pyrope content through the average number, n, of Mg-cations on the six dodecahedral sites surrounding a SiO_4-tetrahedron:

$$n = \frac{1}{6}\sum_i Z_i P_i \qquad (2)$$

where P_i is the measured relative intensity of resonance i and Z_i is the number of Mg cations corresponding to the configuration of resonance i (e.g., $Z_i = 6$ for MgMg-MgMgMgMg, $Z_i = 5$ for MgCa-MgMgMgMg and MgMg-MgMgMgCa, etc.).

For resonances corresponding to more than one configuration, Z_i is taken to be the mean number of Mg cations based on the ratios of their expected probabilities for a random distribu-

TABLE 3. Relative peak intensities of the NMR spectra and comparison with statistical probabilities relating to complete Mg-Ca disorder

Si configuration			Py85-1000				Py85-1200a			
			Observed intensity		Statistical probability*		Observed intensity		Statistical probability	
First Shell	Second Shell	Position (ppm)	Area (%)	FWHM (ppm)	X_{Mg}^{MP} = 0.844 (%)	X_{Mg}^{NMR} = 0.850 (%)	Area (%)	FWHM (ppm)	X_{Mg}^{MP} = 0.848 (%)	X_{Mg}^{NMR} = 0.862 (%)
MgMg	MgMgMgMg	–72.2	40.5	0.60	36.6	38.1	42.8	0.52	37.6	41.7
	MgMgMgCa	–73.4	22.2	0.63	27.1	26.9	23.2	0.54	27.0	26.5
	MgMgCaCa	–74.5	6.1	0.64	7.5	7.1	5.6	0.52	7.3	6.3
MgCa	MgMgMgMg +									
MgMg	MgCaCaCa	–75.6	14.3	0.70	14.5	14.3	14.5	0.62	14.3	13.9
MgCa	MgMgMgCa +									
MgMg	CaCaCaCa	–76.7	9.8	0.75	10.0	9.5	9.3	0.66	9.7	8.4
MgCa	MgMgCaCa	–77.8	4.3	0.90	2.8	2.5	3.9	0.89	2.6	2.0
MgCa	MgCaCaCa +									
CaCa	MgMgMgMg	–78.9	2.7	1.00	1.6	1.5	0.8	0.61	1.5	1.3

* For better comparison with the observed intensities, the statistical probabilities were normalized, so that the sum of probabilites of the fitted configurations equals 100%.

TABLE 3—*Continued*

Si configuration			Py85-1200				Py85-1400			
			Observed intensity		Statistical probability*		Observed intensity		Statistical probability	
First Shell	Second Shell	Position (ppm)	Area (%)	FWHM (ppm)	X_{Mg}^{MP} = 0.849 (%)	X_{Mg}^{NMR} = 0.856 (%)	Area (%)	FWHM (ppm)	X_{Mg}^{MP} = 0.842 (%)	X_{Mg}^{NMR} = 0.875 (%)
MgMg	MgMgMgMg	–72.2	41.5	0.52	37.9	39.7	46.4	0.53	36.1	44.9
	MgMgMgCa	–73.4	23.1	0.54	26.9	26.7	22.9	0.54	27.1	25.9
	MgMgCaCa	–74.5	5.6	0.55	7.2	6.7	5.0	0.55	7.6	5.6
MgCa	MgMgMgMg +									
MgMg	MgCaCaCa	–75.6	14.4	0.63	14.3	14.1	13.6	0.61	14.5	13.5
MgCa	MgMgMgCa +									
MgMg	CaCaCaCa	–76.7	9.4	0.67	9.6	9.0	8.7	0.72	10.2	7.5
MgCa	MgMgCaCa	–77.8	4.1	0.94	2.6	2.3	2.5	0.97	2.9	1.6
MgCa	MgCaCaCa +									
CaCa	MgMgMgMg	–78.9	1.9	1.00	1.5	1.4	0.8	0.99	1.6	1.1

TABLE 3—*Continued*

Si configuration			Py85-1400b				Py75-1000			
			Observed intensity		Statistical probability*		Observed intensity		Statistical probability	
First Shell	Second Shell	Position (ppm)	Area (%)	FWHM (ppm)	X_{Mg}^{MP} = 0.844 (%)	X_{Mg}^{NMR} = 0.855 (%)	Area (%)	FWHM (ppm)	X_{Mg}^{MP} = 0.741 (%)	X_{Mg}^{NMR} = 0.777 (%)
MgMg	MgMgMgMg	–72.2	41.5	0.55	36.6	39.5	25.1	0.62	16.9	22.2
	MgMgMgCa	–73.4	22.8	0.58	27.1	26.8	21.1	0.64	23.6	25.5
	MgMgCaCa	–74.5	5.3	0.54	7.5	6.8	8.3	0.63	12.4	11.0
MgCa	MgMgMgMg +									
MgMg	MgCaCaCa	–75.6	14.3	0.66	14.5	14.2	16.1	0.71	14.7	14.9
MgCa	MgMgMgCa +									
MgMg	CaCaCaCa	–76.7	9.7	0.73	10.0	9.1	15.2	0.79	16.7	14.8
MgCa	MgMgCaCa	–77.8	4.3	1.00	2.8	2.3	8.0	0.82	8.6	6.3
MgCa	MgCaCaCa +									
CaCa	MgMgMgMg	–78.9	2.1	1.00	1.6	1.4	3.4	0.82	4.1	3.0
MgCa	CaCaCaCa +									
CaCa	MgMgMgCa	–80.0					2.8	1.00	3.1	2.2

TABLE 3—*Continued*

Si configuration			Py75-1200				Py75-1400			
			Observed intensity		Statistical probability*		Observed intensity		Statistical probability	
First Shell	Second Shell	Position (ppm)	Area (%)	FWHM (ppm)	X_{Mg}^{MP} = 0.749 (%)	X_{Mg}^{NMR} = 0.761 (%)	Area (%)	FWHM (ppm)	X_{Mg}^{MP} = 0.747 (%)	X_{Mg}^{NMR} = 0.761 (%)
MgMg	MgMgMgMg	–72.2	21.1	0.66	18.0	19.7	20.4	0.63	17.7	19.7
	MgMgMgCa	–73.4	21.0	0.65	24.1	24.7	22.1	0.66	23.9	24.7
	MgMgCaCa	–74.5	9.6	0.66	12.1	11.7	9.1	0.61	12.2	11.7
MgCa	MgMgMgMg +									
MgMg	MgCaCaCa	–75.6	15.8	0.77	14.7	14.8	15.4	0.74	14.7	14.8
MgCa	MgMgMgCa +									
MgMg	CaCaCaCa	–76.7	16.2	0.81	16.4	15.7	17.5	0.83	16.5	15.7
MgCa	MgMgCaCa	–77.8	9.8	0.90	8.1	7.3	8.1	0.75	8.2	7.3
MgCa	MgCaCaCa +									
CaCa	MgMgMgMg	–78.9	4.0	0.89	3.8	3.5	4.0	0.88	3.9	3.5
MgCa	CaCaCaCa +									
CaCa	MgMgMgCa	–80.0	2.5	1.00	2.9	2.6	3.4	1.00	2.9	2.6

tion, I_{STAT}, calculated with their nominal compositions (i.e., X_{Mg} = 0.85 or = 0.75). Thus, for the resonance at –75.6 ppm, $\mathcal{Z}$ is given by:

$$\mathcal{Z}(-75.6\text{ppm}) = \left(\frac{3 \cdot I_{STAT}^{MgMg\text{-}MgCaCaCa} + 5 \cdot I_{STAT}^{MgCa\text{-}MgMgMgMg}}{I_{STAT}^{MgMg\text{-}MgCaCaCa} + I_{STAT}^{MgCa\text{-}MgMgMgMg}} \right) \quad (3)$$

For composition $Py_{85}Gr_{15}$, a value of $\mathcal{Z}$(–75.6 ppm) = 4.883 is obtained; for $Py_{75}Gr_{25}$, $\mathcal{Z}$(–75.6 ppm) = 4.636 ia obtained. For the resonance at –76.7 ppm, $\mathcal{Z}_1$ is given by:

$$\mathcal{Z}(-76.7\text{ppm}) = \left(\frac{2 \cdot I_{STAT}^{MgMg\text{-}CaCaCaCa} + 4 \cdot I_{STAT}^{MgCa\text{-}MgMgMgCa}}{I_{STAT}^{MgMg\text{-}CaCaCaCa} + I_{STAT}^{MgCa\text{-}MgMgMgCa}} \right). \quad (4)$$

For $Py_{85}Gr_{15}$, a value of $\mathcal{Z}$(–76.7 ppm) = 3.992 is obtained; for $Py_{75}Gr_{25}$ a value of $\mathcal{Z}$(–76.7 ppm) = 3.973 is obtained. The resulting compositions computed from the NMR spectra are up to 3% X_{Mg} higher than those determined by microprobe analysis (Table 3). The calculation of the average pyrope content (X_{Mg}^{NMR}) from the NMR data takes only the seven or eight resonances into account which are observable and, hence, those fitted in the spectra. Thus, the Ca-rich configurations at smaller chemical shift values were neglected. Although these Ca-rich configurations are not observed, they could nevertheless be present, which would bias the NMR towards more Mg-rich compositions. As discussed in the experimental section, the limit of detection of resonances in ^{29}Si NMR spectra is about 1%. If we allow a relative intensity of up to 1% for each of the different Ca-rich configurations which were not fitted, X_{Mg}^{NMR} decreases and agrees with the compositions determined by microprobe analysis. The average pyrope contents calculated from the NMR-spectra (X_{Mg}^{NMR}) represent therefore maximum values. This needs to be emphasized because in most spectra there is some weak, poorly resolved intensity in the range between –80 and –83 ppm which is not reported in Table 3. This is particularly evident in the fit of Py85-1000 (Fig. 3), which shows a distinct positive deviation in the residual plot near –80 ppm. Including those intensities into the determination of the garnet compositions typically makes X_{Mg}^{NMR} about 0.5 mol% more calcic. Hence, neglecting this poorly resolved intensity of the Ca-rich configurations does not significantly change the composition and therefore the conclusions concerning the state of order are not affected.

None of the garnets investigated has a completely random Ca-Mg distribution based on a comparison of the fitted peak intensities with the statistical probabilities corresponding to hypothetical disorder (Table 3). This is demonstrated by considering the two most intense resonances at –72.2 and –73.4 ppm. The measured relative intensities of the resonances corresponding to MgMg-MgMgMgMg and to MgMg-MgMgMgCa match the calculated random distribution model to within ±5%. The agreement between observed intensities and the random model probabilities is better for the compositions computed from the NMR spectra than for those obtained by microprobe analysis. However, in both garnet compositions the measured intensity of the resonance corresponding to the configuration MgMg-MgMgMgMg is always larger than that calculated assuming a random distribution, regardless of whether the measured or apparent composition is used. Also, the intensity of the resonance corresponding to the configuration MgMg-MgMgMgCa is always less than the calculated one. For these peaks, the differences between fitted and calculated intensity are larger than the experimental and fitting uncertainties. Furthermore, constraining the relative intensities to those for a random distribution (allowing all other parameters to vary freely) produces very poor fits to the experimental spectra. The configuration MgMg-MgMgMgMg is energetically preferred over MgMg-MgMgMgCa. This observation also holds for the pyrope-rich garnets investigated previously (Bosenick et al. 1995).

A garnet of composition $Py_{85}Gr_{15}$ with a totally random distribution of Ca and Mg should display relative peak intensities of 38.1 and 26.9% for the two strongest resonances at –72.2 and –73.4 ppm (Table 3). In the NMR spectra of the $Py_{85}Gr_{15}$ samples synthesized at 1000 and 1200 °C and that of the sample B005 synthesized at 1400 °C (spectrum Py85-1400b), the resonance at –72.2 ppm has an average relative intensity of 41 ± 1.8% and the second strongest peak an average relative intensity of 22 ± 1.2%. In the spectrum Py85-1400 recorded on sample B018 a greater mismatch between the observed and calculated peak intensities is seen (Table 3). This sample seems, therefore, to have a more ordered state than those synthesized at lower temperatures. This is difficult to explain, because ordering should decrease with increasing temperature of synthesis unless, as will be dicussed in more detail below, it was quenched more slowly than the other samples.

The relative occupancy of the MgMg-MgMgMgMg configuration compared to that of MgMg-MgMgMgCa can be expressed by an intensity ratio (Fig. 6). For composition $Py_{85}Gr_{15}$, ratios between 1.75 and 1.95 were obtained for the different syntheses depending upon the different peak shapes used in the fits of the spectra. A higher ratio of 2.15 is found for sample B018 synthesized at 1400 °C. A totally random distribution of Mg and Ca gives a ratio of 1.42 and a compositional uncertainty of ± 1 mol% would correspond to the range between 1.31 and 1.54 (Fig. 6). The measured ratios of 1.75, 1.95, and 2.15 at the three different temperatures would require garnet compositions of X_{Mg} = 0.875, X_{Mg} = 0.886, and X_{Mg} = 0.896 respectively, if compositional variation between the samples was to be responsible for the observed variations (Fig. 6). The microprobe analyses (on deposit as stated previously) rule out this possibility. The possible presence of about 1 mol% pyroxene in the sample synthesized at 1000 °C can explain only a compositional change in the garnet to X_{Mg} = 0.858. Instead, the measured resonance intensities indicate a slight tendency towards Mg-Ca order.

Similar evidence for short-range order of Mg and Ca is observed in $Py_{75}Gr_{25}$ compositions, and its temperature dependence could be experimentally obtained. For a random cation distribution, the probability is greatest for the configuration MgMg-MgMgMgCa and second greatest for the configuration MgMg-MgMgMgMg. However, in $Py_{75}Gr_{25}$ synthesized at 1000 °C the resonance assigned to the configuration MgMg-MgMgMgMg has a greater intensity than that of MgMg-MgMgMgCa. The same observation was made for a $Py_{75}Gr_{25}$ sample synthesized at 1100 °C (Bosenick et al. 1995). In the case of $Py_{75}Gr_{25}$ synthesized at 1200 °C, the configurations MgMg-MgMgMgMg and MgMg-MgMgMgCa are equally occupied and in $Py_{75}Gr_{25}$ synthesized at 1400 °C,

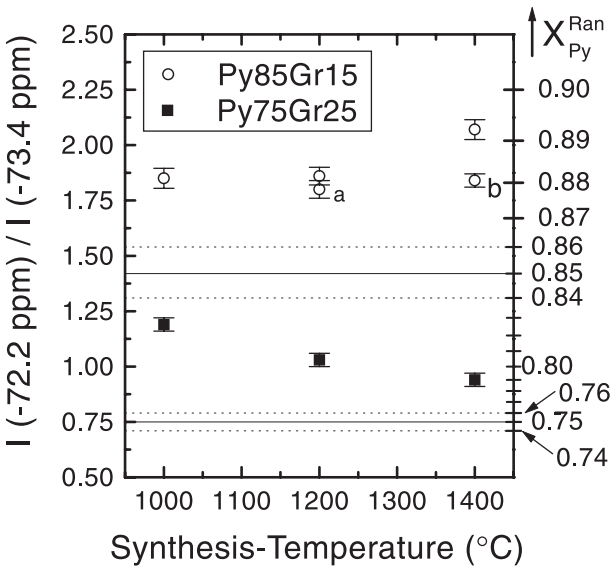

FIGURE 6. Ratioed intensities of the two configurations MgMg-MgMgMgMg and MgMg-MgMgMgCa, i.e., resonances at –72.2 and –73.4 ppm, as a function of synthesis temperature. The labeling within the plot refers to Table 1. The error bars give the changes in the intensity ratios when peak shapes used in peak-fitting procedure are varied between 100% Gaussian and 100% Lorentzian line shape. The Y-axis to the right gives the pyrope-content, which in the case of total random cation disorder corresponds to the intensity ratios given on the left-hand axis. Assuming an uncertainty of ± 1 mol% in the determined compositions, the intensity ratio of the $Py_{85}Gr_{15}$ samples should plot between the dotted lines around $X_{Py}^{RAN} = 0.85$ and those of compositions $Py_{75}Gr_{25}$ between the dotted lines around $X_{Py}^{RAN} = 0.75$, if Mg and Ca were totally disordered. However, the observed intensity ratios deviate too much from these areas to be explained solely by errors in composition and hence, indicate the presence of short-range order.

the latter configuration is slightly preferred. Hence, disorder tends to increase with increasing synthesis temperature, but a complete random distribution of Ca and Mg is not observed in any of the samples.

Again, the relative occupancies of the configurations MgMg-MgMgMgMg and MgMg-MgMgMgCa can be compared. Their intensity ratios decrease systematically from 1.20 to 0.925 with increasing synthesis temperature (Fig. 6). A ratio of 0.75 is calculated for a $Py_{75}Gr_{25}$ sample having a totally random distribution of Mg and Ca. Ratios of 1.2, 1.0, and 0.925, as measured from the spectra of the samples synthesized at 1000, 1200, and 1400 °C, respectively, would require pyrope mole fractions of $X_{Mg} = 0.827$, $X_{Mg} = 0.802$, and $X_{Mg} = 0.787$, if the samples were disordered (Fig. 6). This is not supported by the microprobe analyses. The presence of up to 3 mol% of pyroxene in the spectrum Py75-1000 can only account for a change in composition to $X_{Mg} = 0.773$. Hence, only short-range order can explain the differences in the spectra rather than deviations from the nominal starting compositions.

DIFFUSION AND INTERPRETATION OF SPECTRA

The samples may not represent the *P-T* conditions of synthesis. Ordering due to inherited compositional inhomogenities in the glasses can be ruled out, but the observed degrees of order could be a function of the quench rate and/or the synthesis time. The differences in the spectra of the two $Py_{85}Gr_{15}$ syntheses at 1400 °C suggest that differences in quench rates could play a role, because the experimental conditions were identical in both experiments. The fact that, in the case of the $Py_{85}Gr_{15}$ composition, the biggest differences in the spectra are found in garnets synthesized at the highest temperatures could be a result of ordering occurring upon quenching. The dodecahedra in garnet share edges with one another and hence, an exchange of Ca and Mg should be relatively easy. We calculated the jump time needed for Ca and Mg atoms to change places between nearest dodecahedral sites using the Einstein-Smoluchowski relation (e.g., Atkins 1978). This is given as:

$$D = \frac{x^2}{2 \cdot t} \tag{5}$$

where D is the diffusion coefficient, x the jump length, and t the jump time. The diffusion coefficient, D, was determined by applying the Arrhenius equation:

$$D = D_0 \cdot \exp\left(\frac{E_A}{\mathrm{R} \cdot T}\right) \tag{6}$$

where the activation energy, E_A, and the frequency parameter, D_0, were taken from experimental studies on the self-diffusion of Mg and Ca in pyrope and grossular, respectively (Schwandt et al. 1995 and 1996). The Mg cations have a short calculated jump time down to about 1100 °C (Table 4). Even at 1000 °C, the jump time of Mg is short enough to allow for a movement of the Mg cations within our quench times. Changes in the ordering state should be hindered, however, by the much slower diffusing Ca cations, which have jump times that are about two orders of magnitude slower. Hence, the more Ca-rich the garnets, the more likely that their high-temperature ordering state can be preserved upon quenching. In the more Mg-rich $Py_{85}Gr_{15}$ solid solution, where an almost identical ordering state was observed independent of synthesis temperature, it is possible that cation movements took place during the quench process. The $Py_{85}Gr_{15}$ sample synthesized at 1100 °C (Bosenick et al. 1995) has a slightly greater degree of short-range order compared to those studied herein. This sample was synthesized in a different laboratory than those of this study. It is possible that the quenching rate was faster due to differences in the experimental setup.

Both solid-solution compositions $Py_{85}Gr_{15}$ and $Py_{75}Gr_{25}$ show small deviations from totally random mixing of Mg and Ca. It was shown that the degree of order is not dependent on the glass starting material used for the garnet synthesis (compare $Py_{85}Gr_{15}$ synthesized at 1200 °C from glasses melted 1, 2, and 3 times, Table 3). It was also shown that the observed deviations from random Ca and Mg mixing are too large to be solely explained by compositional deviations from the nominal com-

TABLE 4. Diffusion times*

T (K)	Time (s)	
	Mg	Ca
1273	7.29	200.48
1473	0.16	27.45
1673	0.01	6.05

* Calculated for Mg and Ca cations in a pyrope-rich garnet to jump to an adjacent dodecahedral site over a distance of ~3.55 Å.

positions (Fig. 6). It follows, therefore, that a preference for the pyrope-like configuration MgMg-MgMgMgMg relative to MgMg-MgMgMgCa has to be coupled to an additional preference for more Ca-rich configurations, if bulk composition is to be maintained. However, in the pyrope-rich solid-solutions Ca-rich configurations are statistically small. The corresponding NMR resonances could therefore not be observed and the expected increase in occupation of more Ca-rich configurations can not be established and/or quantified. A preference for Mg-rich configurations, on the one hand, and Ca-rich configurations, on the other, indicates that short-range ordering in pyrope-grossular solid solutions is characterized by Mg-rich and Ca-rich clusters.

The effect of this clustering on the configurational entropy (S_c) can be approximated by using the measured ^{29}Si peak intensities in a cluster-variation model (Appendix 1). Various methods were used to account for the intensity of the Ca-rich configurations that could not be observed by NMR due to their presumably low populations (Appendix 2). Except for sample Py75-1000 and Py85-1400, the calculated S_c differed from those for a random distribution by less than 1 J/mol·K. A very small additional entropy effect arises if Ca-clustering, similar to that measured for the Mg-rich configurations, is presumed to be present, due to the low populations of these configurations. Py75-1000 and Py85-1400 show a greater entropy decrease of about 2–3 J/mol·K. This is primarily a consequence of the larger difference between the apparent and measured compositions. Hence, compared to the random distribution more Ca-rich configurations, which were not observed by NMR, are required to match the apparent with the measured composition (see Appendix 2).

Knowing that different structural states can be quenched in from high temperatures and pressures, it must be considered if variations in the unit-cell dimension and diffraction line width changes are related to order/disorder or cluster formation. There has been a number of studies on the volumes of mixing of synthetic pyrope-grossular garnets (e.g., Newton et al. 1977; Delany 1981; Wood 1988). There is large scatter between the different data sets and it has been difficult to describe the exact behavior of the volumes of mixing. A more recent X-ray diffraction investigation (Ganguly et al. 1993) removed many of the uncertainties and an asymmetric mixing model is supported by the most recent experimental results (Bosenick and Geiger 1997). Complications are probably, however, still present. Ganguly et al. (1993) describe one grossular-rich sample (X_{Mg} = 0.151) having an "anomalously" large unit-cell dimension compared to those of the other solid solutions. Although they checked this sample for impurities and compositional inhomogenities, they were unable to give an explanation for its "anomalous" behavior. Similarly, in the study of Bosenick and Geiger (1997) a garnet of composition $Py_{75}Gr_{25}$ gave a unit-cell dimension relatively small compared to other compositions. In the case of the latter garnet, it is known that a certain degree of short-range order is present. Moreover, it is possible that the former garnet has a structural state different compared to the other solid solution compositions. Indeed, the garnets studied by Ganguly et al. (1993) were synthesized over a range of temperatures from 1000 to 1400 °C. The garnet of composition X_{Mg} = 0.151 was grown at 1000 °C and could have a relatively high degree of Ca-Mg order. Hence, the differences between the various studies on molar volumes could be related to different structural states between the garnets investigated. With regard to the presence of diffraction peak broadening, we consider it to be partially related to fluctuations in structural state, as well as to compositional heterogeneity. Correspondingly, lower temperature syntheses (i.e., 1000 °C) show significantly broader diffraction lines compared to those synthesized at 1400 °C.

ACKNOWLEDGMENTS

This work has been supported by the "Deutsche Forschungsgemeinschaft", grant number Ge 649/2-3, as part of a priority program concerning element partitioning in rock-forming silicates. We would like to thank the "Bayerische Geoinstitut" in Bayreuth where most of the garnet syntheses were performed and Director David Rubie. Without their generosity this study could not have been realized. We also want to acknowledge the advice and help in the synthesis experiments of M. Rauch, V. von Seckendorff, G. Hermansdörfer (Bayreuth) and A. Stahl and H. Voigtländer (Kiel). The NMR equipment at UCD was provided by the W.M. Keck Foundation. We appreciate the constructive reviews by B.L. Sherriff, M.J. Holdaway and an anonymous referee which helped to improve the presentation.

REFERENCES CITED

Ackermann, L., Cemič, L., and Langer K. (1983) Hydrogarnet substitution in pyrope — a possible location for water in the mantle. Earth and Planetary Science Letters, 63, 208–214.

Atkins, P.W. (1978) Physical Chemistry, p. 1018. Oxford University Press, U.K.

Azaroff, L.V. and Buerger, M.J. (1958) The powder method in X-ray crystallography, p. 342. McGraw-Hill Book Company, New York.

Bosenick, A. and Geiger, C.A. (1997) Powder diffraction study of synthetic pyrope-grossular garnets between 20 and 295 K. Journal of Geophysical Research. Solid Earth, 102 (B-10), 22649–22657.

Bosenick, A., Geiger, C.A., Schaller, T., and Sebald, A. (1995) An ^{29}Si MAS NMR and IR spectroscopic investigation of synthetic pyrope-grossular garnet solid solutions. American Mineralogist, 80, 691–704.

Cheng, W., Greenwood, H.J., Hu, H., and Frost, D.C. (1990) XRD and XPS analyses of the grossular-hydroglossular series. Canadian Mineralogist, 28, 87–91.

Delany, J.M.(1981) A spectral and thermodynamic investigation of synthetic pyrope-grossular garnets, Ph. D. dissertation, p. 186. University of California, Los Angeles.

de Fontaine, D. (1979) Configurational thermodynamics of solid solutions. Solid State Physics, 34, 73–274.

Ganguly, J., Cheng, W., and O'Neill, H.St.C. (1993) Syntheses, volume, and structural changes of garnets in the pyrope-grossular join: Implications for stability and mixing properties. American Mineralogist, 78, 583–593.

Geiger, C.A., Langer, K., Bell, D.R., Rossmann, G.R., and Winkler, B. (1991) The hydroxide component in synthetic pyrope. American Mineralogist, 76, 46–59.

Kirkpatrick, R.J., Oestrike, R., Weiss, C.A., Smith, K.A., and Oldfield, E. (1986) High resolution ^{27}Al and ^{29}Si NMR spectroscopy of glasses and crystals along the join $CaMgSi_2O_6$-$CaAl_2Si_2O_6$. American Mineralogist, 71, 705–711.

Newton, R.C., Charlu, T.V., and Kleppa, K.M. (1977) Thermochemistry of high pressure garnets and clinopyroxenes in the system CaO-MgO-Al_2O_3-SiO_2. Geochim. Cosmochim. Acta, 41, 369–377.

Press, W.H., Flannery, B.P., Teukolsky, S.A., and Vetterling, W.T. (1986) Numerical recipes, the art of scientific computing, 818 p. Cambridge University Press, Cambridge, New York.

Schwandt, C.S., Cygan, R.T., and Westrich, H.R. (1995) Mg self-diffusion in pyrope garnet. American Mineralogist, 80, 483–490.

———(1996) Ca self-diffusion in grossular garnet. American Mineralogist, 81, 448–451.

Sobolev, N.V. Jr., Kuznetsova, I.K., and Zyuzin, N. (1968) The petrology of grosspydite xenoliths from the Zagadochnaya kimberlite pipe in Yakutia. Journal of Petrology, 9, 253–280.

Weber, K. (1991) Pulver 91—Ein Programm zur Auswertung von Pulverdiffraktogrammen, Institut fuer Mineralogie und Kristallographie, TU-Berlin.

Withers, A.C., Wood, B.J., and Carroll, M.R. (1998) The OH content of pyrope at high pressure. Chemical Geology, 147, 161–171.

Wood, B.J. (1988) Activity measurements and excess entropy-volume relationships for pyrope-grossular garnets. Journal of Geology, 96, 721–729.

MANUSCRIPT RECEIVED OCTOBER 9, 1998
MANUSCRIPT ACCEPTED MARCH 25,1999
PAPER HANDLED BY JONATHAN F. STEBBINS

APPENDIX 1: CALCULATION OF CONFIGURATIONAL ENTROPY FROM ^{29}Si NMR SPECTRA

Although Ca and Mg occupy a single crystallographic site, short-range order can produce a non-random Ca-Mg distribution and affect the free energy of the garnet through a reduction of the configurational entropy (S_c) of Ca-Mg mixing. Such short-range order can be observed as a deviation from a random distribution of the configurations within the six dodecahedral sites that share oxygens with the Si tetrahedron. Thus, the ^{29}Si NMR spectra give information on the populations of clusters of six dodecahedral sites (6-clusters). For low degrees of order, the reduction of S_c can be calculated from the population of the 6-clusters centered about the Si position using cluster-varation techniques (e.g., Fontaine 1979). Because adjacent 6-clusters share only two corner-linked dodecahedra, the configurational entropy is given approximately by:

$$S_{C,NMR} = 3R(-\Omega_6 + 5\Omega_1) \quad \text{(A1)}$$

where Ω_6 is the number of configurations of 6-clusters, given by:

$$\Omega_6 = \sum_k m_k p_k \ln(p_k) \quad \text{(A2)}$$

in which k runs over the fifteen possible ways of distributing Ca and Mg around the Si-position, p is the probability of a given configuration and m is its multiplicity. For example, for a random distribution, the environment MgCa-MgMgMgCa has a probability $p = X_{Mg}^4(1-X_{Mg})^2$ and multiplicity m = 8. The term Ω_1 corresponds to the number of configurations contained in the point cluster (i.e., mixing of Ca and Mg on a single crystallographic position), given by:

$$\Omega_1 = X_{Mg}\ln(X_{Mg}) + (1-X_{Mg})\ln(1-X_{Mg}) \quad \text{(A3)}$$

where X_{Mg} is the mole fraction of pyrope. For a random distribution containing no short-range order, the configurational entropy is given by the regular-solution model in the Bragg-Williams approximation:

$$S_{C,BW} = 3R(-\Omega_1) \quad \text{(A4)}$$

Comparison of $S_{C,NMR}$ with $S_{C,BW}$ gives the entropic contribution from any observed short-range Ca-Mg order.

APPENDIX 2: CONFIGURATIONAL ENTROPY CALCULATION FOR PY-GR GARNETS

The following models were combined with the results of Appendix 1 to estimate the configurational entropy due to short range order consistent with the ^{29}Si NMR spectra:

Model 0: No short-range order is assumed, S_C is calculated from Equations A3 and A4 using the EMP results for the composition.

Model 1: Populations of Mg-Ca configurations are obtained from ^{29}Si NMR spectra and the apparent compositions are calculated from this distribution. All apparent compositions obtained this way are more Mg-rich than the EMP results, possibly due to unobserved peaks arising from Ca-rich sites.

Model 2: Same as Model 1, except that the intensities of the "unobserved" Ca-rich sites (CaCa-CaCaCaCa, CaCa-MgCaCaCa and CaCa-MgMgCaCa for Py75; these sites plus CaCa-MgMgMgCa and MgCa-CaCaCaCa for Py85) are assumed to be the same as for the random distribution of Model 0. Apparent composition calculated from this distribution is used in the entropy calculation.

Model 3: Populations of Mg,Ca configurations obtained from the ^{29}Si NMR spectra, with intensity of the "unobserved" Ca-rich sites listed for Model 2 adjusted to make the apparent composition calculated from the site populations equal to that obtained from EMP data. The ratios of the unobserved Ca-rich sites are the same as for the random distribution of Model 0.

Model 4: Same as Model 3, except that the ratios of the Ca-rich sites (CaCa-CaCaCaCa, CaCa-MgCaCaCa, and CaCa-MgMgCaCa) are adjusted to mimic the ordering pattern observed for the converse Mg-rich sites (increase of CaCa-CaCaCaCa and MgMg-MgMgMgMg), fractional decrease of CaCa-MgCaCaCa and CaCa-MgMgCaCa relative to the random distribution similar to that of MgMg-MgMgMgCa and MgMg-MgMgCaCa.

APPENDIX 2,TABLE 1. Results of configurational entropy calculations and assumed population of unobserved Ca-rich sites

Sample	X_{Mg}	$S_{C,BW}$*	$S_{C,NMR}$	X_{Mg}	$S_{C,BW}$*	$S_{C,NMR}$	X_{Mg}	$S_{C,BW}$*	$S_{C,NMR}$	X_{Mg}	$S_{C,BW}$*	$S_{C,NMR}$
	Py85-1000			**Py85-1200a**			**Py85-1200**			**Py85-1400**		
Model 0	0.844	10.8	10.8	0.848	10.6	10.6	0.849	10.6	10.6	0.842	10.9	10.9
Model 1	0.850	10.5	9.9	0.862	10.0	9.5	0.856	10.3	9.7	0.875	9.4	9.1
(I_4,I_3,I_2,I_1,I_0)†	(0.0, 0.0, 0.0, 0.0, 0.0)			(0.0, 0.0, 0.0, 0.0, 0.0)			(0.0, 0.0, 0.0, 0.0, 0.0)			(0.0, 0.0, 0.0, 0.0, 0.0)		
Model 2	0.846	10.7	10.4	0.857	10.2	9.9	0.852	10.4	10.2	0.869	9.7	9.5
(I_4,I_3,I_2,I_1,I_0)	0.01, 0.91, 0.25, 0.03, 0.001)			(0.01, 0.86, 0.23, 0.03, 0.001)			(0.01, 0.84, 0.23, 0.03, 0.001)			(0.02, 0.94, 0.27, 0.03, 0.002)		
Model 3	0.844	10.8	10.4	0.848	10.6	9.9	0.849	10.6	10.3	0.842	10.9	8.4
(I_4,I_3,I_2,I_1,I_0)	(0.02, 1.20, 0.34, 0.04, 0.002)			(0.04, 2.60, 0.69, 0.08, 0.004)			(0.02, 1.40, 0.37, 0.04, 0.02)			(0.10, 5.75 ,1.62, 0.20, 0.01)		
Model 4	0.844	10.8	10.4	0.848	10.6	9.9	0.849	10.6	10.2	0.842	10.9	8.1
(I_4,I_3,I_2,I_1,I_0)	(0.02, 1.20, 0.27, 0.03, 0.07)			(0.04, 2.50, 0.52, 0.07, 0.16)			(0.02, 1.35, 0.28, 0.04, 0.02)			(0.10, 5.44, 1.02, 0.16, 0.55)		
	Py85-1400b			**Py75-1000**			**Py75-1200**			**Py75-1400**		
Model 0	0.844	10.8	10.8	0.741	14.3	14.3	0.749	14.1	14.1	0.747	14.1	14.1
Model 1	0.855	10.3	9.7	0.777	13.2	12.6	0.761	13.7	13.1	0.761	13.7	13.2
(I_4,I_3,I_2,I_1,I_0)†	(0.0, 0.0, 0.0, 0.0, 0.0)			(0, 0, 0)			(0, 0, 0)			(0, 0, 0)		
Model 2	0.850	10.5	10.2	0.768	13.5	13.1	0.753	13.9	13.7	0.753	14.0	13.8
(I_4,I_3,I_2,I_1,I_0)	(0.02, 0.91, 0.25, 0.03, 0.001)			(1.48, 0.35, 0.03)			(1.3, 0.30, 0.03)			(1.37, 0.31, 0.03)		
Model 3	0.844	10.8	10.3	0.741	14.3	12.4	0.749	14.1	13.8	0.747	14.1	13.8
\(I_4,I_3,I_2,I_1,I_0)	(0.04, 2.05, 0.57, 0.07, 0.003)			(5.97, 1.39, 0.12)			(2.03, 0.45, 0.04)			(2.36, 0.53, 0.05)		
Model 4	0.844	10.8	10.2	0.741	14.3	11.8	0.749	14.1	13.6	0.747	14.1	13.6
(I_4,I_3,I_2,I_1,I_0)	(0.03, 1.96, 0.39, 0.06, 0.17)			(3.46, 1.07, 1.8)			(1.47, 0.36, 0.43)			(1.57, 0.44, 0.56)		

* All entropy values given in units (J/mol·K).
† Assumed intensities (percent) for unobserved Ca rich sites: for Py85 and Py75, I_4 = CaCa-CaCaCaCa; I_1 = CaCa-MgCaCaCa; I_2 = CaCa-MgMgCaCa; and in addition for Py85, I_3 = CaCa-MgMgMgCa and I_4 = MgCa-CaCaCaCa.